LC/UV/HRAM MS-based impurity profiling and structure elucidation of phosphoramidite raw materials used for oligonucleotide synthesis

Authors

Sven Hackbusch[1], Gary Held[2], Yi Zhang[3], Min Du[4]

Thermo Fisher Scientific
[1]San Jose, CA, USA
[2]Milwaukee, WI, USA
[3]Philadelphia, PA, USA
[4]Boston, MA, USA

Keywords

Phosphoramidites, pharmaceutical raw materials, oligonucleotide synthesis, impurity identification, structure elucidation, Orbitrap Exploris 120 mass spectrometer, high-resolution accurate mass (HRAM), Vanquish Horizon UHPLC system, Compound Discoverer software

Application benefits

- Sensitive detection of phosphoramidite raw material and related impurities with LC/UV/HRAM-MS
- Confident structure elucidation of low abundant impurities to enable the determination of their critical/non-critical nature, using HRAM MS^2 data and Thermo Scientific™ Compound Discoverer™ software

Goal

Demonstrate the capability of the Thermo Scientific™ Vanquish™ Horizon UHPLC system combined with the Thermo Scientific™ Orbitrap Exploris™ 120 mass spectrometer to sensitively detect raw material impurities at trace levels and determine their chemical structure based on high-quality MS^2 data using Compound Discoverer software.

Introduction

Solid-phase chemical synthesis based on phosphoramidite chemistry is one of the most employed approaches to synthesize oligonucleotides.[1] With a growing number of therapeutic oligonucleotide compounds in drug development and clinical trials and the complexity of structural modifications introduced, the impurity profiling and analytical control of related starting materials has increased in importance,

as phosphoramidite raw material impurities can directly impact the quality of therapeutic oligonucleotides. As such, it is essential to characterize the impurity profile of these oligonucleotide building blocks and control for them in the manufacturing process.

Impurities can be either reactive or unreactive, critical or noncritical, depending on the type of structural modification present and whether the introduced impurities can be removed in downstream purification steps.[2] Determination of the critical/non-critical nature of impurities based on their structure is a crucial step to ensure high-quality oligonucleotides in the process of drug development and manufacturing.

Regulatory and industry guidance typically requires analytical methods to be able to detect and characterize impurities at levels down to or below 0.1% relative to the authentic raw material.[3] The relative quantitation is usually carried out using UV, whereas the identification and structure elucidation of phosphoramidite impurities relies on mass spectral information.

Here we demonstrate the characterization of phosphoramidite raw materials, i.e., 5'-dimethyloxytrityl-2'-fluoro-N-benzoyl-adenosine cyanoethyl phosphoramidite (5'-DMT-2'-F-A(bz)-CEP, **1**) from different vendors, and the structure elucidation of detected impurities using the Vanquish Horizon UHPLC system coupled with the Orbitrap Exploris 120 mass spectrometer for confident data acquisition and Thermo Scientific™ Chromeleon™ Chromatography Data System (CDS) 7.2.10 and Compound Discoverer 3.3 SP1 software for data analysis.

Experimental

Reagents and consumables

- Water, UHPLC grade, 1 L, Thermo Scientific™ (P/N W8-1)
- Acetonitrile, UHPLC grade, 1 L, Thermo Scientific™ (P/N A956-1)
- Ammonium acetate, Optima™ LC/MS grade, Fisher Chemical™ (P/N A11450)
- Acetonitrile, anhydrous, 99.8+%, Thermo Scientific™ (P/N 042311.AK)
- Thermo Scientific™ SureSTART™ Screw Glass Vial, 2 mL, Level 3 (P/N 6PSV9-1PSS)
- Thermo Scientific™ SureSTART™ 9 mm Screw Caps, Level 3 (P/N 6PSC9TST)

Sample preparation

2' modified RNA phosphoramidites were obtained from four different vendors (referred to as A through D hereafter), with specified purities of 98% or higher. Specifically, the analyzed material in this work was 5'-dimethyloxytrityl-2'-fluoro-N-benzoyl-adenosine cyanoethyl phosphoramidite (5'-DMT-2'-F-A(bz) CEP, **1**), shown in Figure 1.

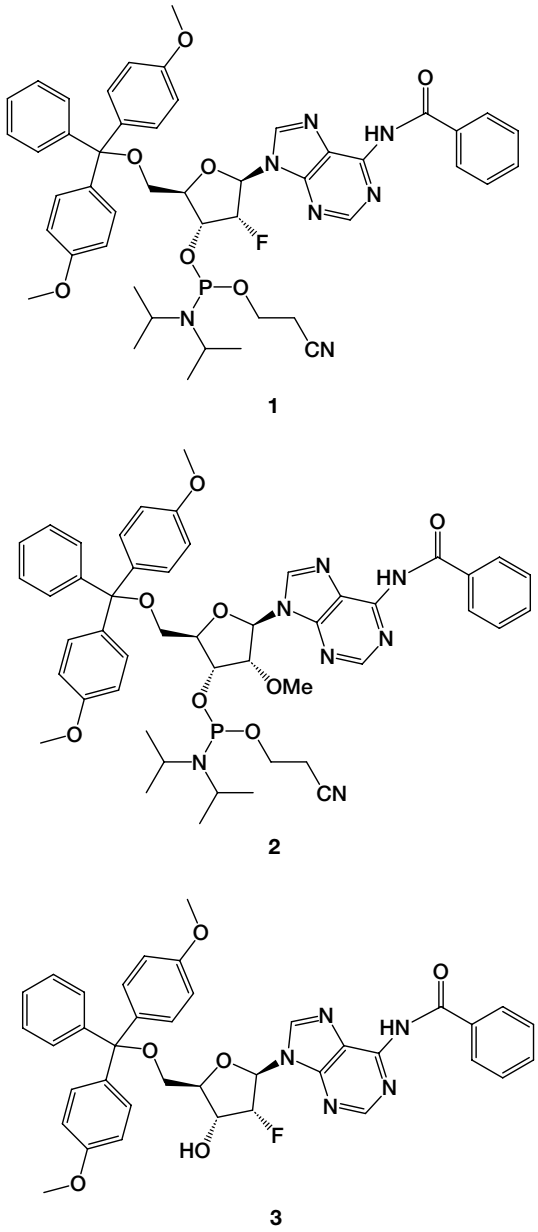

Figure 1. Structure of the 2'-modified RNA phosphoramidites 1 and 2, as well as spiked impurity 3

Working solutions of the different vendors' phosphoramidites were prepared at 1.0 mg/mL by dissolving in anhydrous acetonitrile to avoid oxidation.

To establish the sensitivity of the impurity detection, 5'-dimethyloxytrityl-2'-fluoro-N-benzoyl-adenosine (5'-DMT-2'-F-A(bz), **3**, Thermo Scientific™ P/N J6540203) was spiked into a 1 mg/mL solution of 5'-dimethyloxytrityl-2'-O-methyl-N-benzoyl-adenosine cyanoethyl phosphoramidite (5'-DMT-2'-OMe-A(bz) CEP, **2**) at concentrations of 1 µg/mL (0.1%), 0.1 µg/mL (0.01%), and 10 ng/mL (0.001%).

Sample analysis

Briefly, the LC separation was performed using a Vanquish Horizon UHPLC system, consisting of:

- Vanquish System Base (P/N VF-S01-A-02)
- Vanquish Binary Pump H (P/N VH-P10-A)
- Vanquish Split Sampler HT (P/N VH-A10-A-02)
- Vanquish Column Compartment H (P/N VH-C10-A-03)
- Vanquish Diode Array Detector FG (P/N VF-D11-A-01) with Standard Flow Cell (10 mm, P/N 6083.0510)

This was coupled to a Thermo Scientific Orbitrap Exploris 120 mass spectrometer (P/N BRE725531). The LC/MS analysis was carried out using the following conditions:

Table 1. UHPLC experiment conditions

Parameter	Value
Column	Thermo Scientific™ Accucore™ C18, 2.6 µm, 2.1 × 100 mm (P/N 17126-102130)
Mobile phase	A: 10 mM ammonium acetate in water B: acetonitrile
Flow rate	0.4 mL/min
Column temperature	45 °C (still air mode)
Autosampler temperature	6 °C
Injection volume	2 µL
Needle wash	50% acetonitrile, before and after injection
Mixer volume	35 µL (10 µL static + 25 µL capillary mixer)
Divert valve timing	Flow to waste from 0–1 min and 15.0–20 min
UV detector settings	Wavelength: 254 nm 3D scan: 200–400 nm Data collection rate: 5 Hz

Table 2. UHPLC gradient conditions

Time (min)	Analytical gradient mobile phase B (%)
0.0	30
14.0	95
15.0	95
15.1	30
20.0	30

Mass spectrometry data from the Orbitrap Exploris 120 mass spectrometer was acquired with a Thermo Scientific™ OptaMax™ NG H-ESI ion source. Untargeted impurity characterization experiments on the phosphoramidite samples were carried out using polarity switching Top 2 data-dependent MS^2 ($ddMS^2$) experiments. The MS source conditions, and important MS experiment parameters, are detailed in Tables 3 and 4.

Table 3. MS source conditions

Parameter	Value
Spray voltage	+ 3,250 V / – 2,750 V
Sprayer position	1.5, M/H, center
Vaporizer temperature	325 °C
Ion transfer tube temperature	275 °C
Sheath gas	40 a.u.
Aux gas	10 a.u.
Sweep gas	1 a.u.

Table 4. Polarity switching $ddMS^2$ method parameters

Parameter	Value
MS^1 resolution	60,000 @ *m/z* 200
MS^1 mass range	*m/z* 200–1200
RF level, %	70
Easy-IC	Scan-to-Scan
MS^2 isolation window (*m/z*)	1.5
HCD collision energies (Normalized, %)	10, 20, 40
MS^2 resolution	15,000 @ *m/z* 200
Maximum injection time (ms)	100
Intensity threshold	2.0e5
Dynamic exclusion	Auto

Data processing software

The Thermo Scientific™ Xcalibur™ 4.5 software was used for data acquisition and Thermo Scientific™ FreeStyle™ 1.8 SP2 software for initial data review. Qualitative and quantitative analysis of the UV trace data was carried out in Chromeleon 7.2.10 CDS and Compound Discoverer 3.3 SP1 software was used for spectral deconvolution and peak detection of the LC/MS data, as well as compound identification using an adapted version of the default workflow template "Impurity ID Related and Unknown with Molecular Networks".

Results and discussion

Comprehensive impurity characterization of drug product raw materials requires the detection of impurities that may have different ionization requirements than the raw material itself. The high scan speed of the Orbitrap Exploris 120 mass spectrometer enables rapid data acquisition in both polarities from one injection to accomplish this goal, as previously demonstrated.[4] In this work, data were acquired with polarity switching using Full MS followed by Top2 data-dependent MS^2 acquisition at 60,000 and 15,000 resolution (@ *m/z* 200) for Full MS and MS^2, respectively.

For separation of the raw materials, a 15-minute gradient separation using ammonium acetate buffer and acetonitrile was employed using a solid-core Accucore C18 column, which readily allowed the separation of impurities from the expected compounds. The resulting UV and MS total ion chromatograms for the analysis of one of the phosphoramidite materials are shown in Figure 2 overlaid with a solvent blank injection, showing the separation of the diastereomeric product peaks.

Sensitivity of impurity detection and distinction of isomers by MS^2

To establish the sensitivity of the LC/MS method for the detection of impurities at or below the level typically required, spike-in experiments were carried out using 5'-DMT-2'-F-A(bz) **3**, a potential impurity of 5'-DMT-2'-F-A(bz)-CEP **1** resulting from the loss of the cyanoethyl phosphoramidite group. Since this impurity was already present in the phosphoramidite **1** at detectable levels, it was spiked into a different amidite modality, 5'-DMT-2'-OMe-A(bz)-CEP **2**, at relative concentrations ranging from 0.001% to 0.1%. This was done to model the case of an impurity that was not present in the unspiked sample. The resulting UV traces and ESI(+) XICs from the different injections are shown in Figure 3. As can be seen, impurity **3** eluting at 5.9 min was readily detected down to a relative concentration of 0.01% using the total UV trace, while the 0.001% level was only detected in the mass spectral data. This higher sensitivity of the MS detection may be helpful in monitoring particular impurities of concern or those that do not have a chromophore.

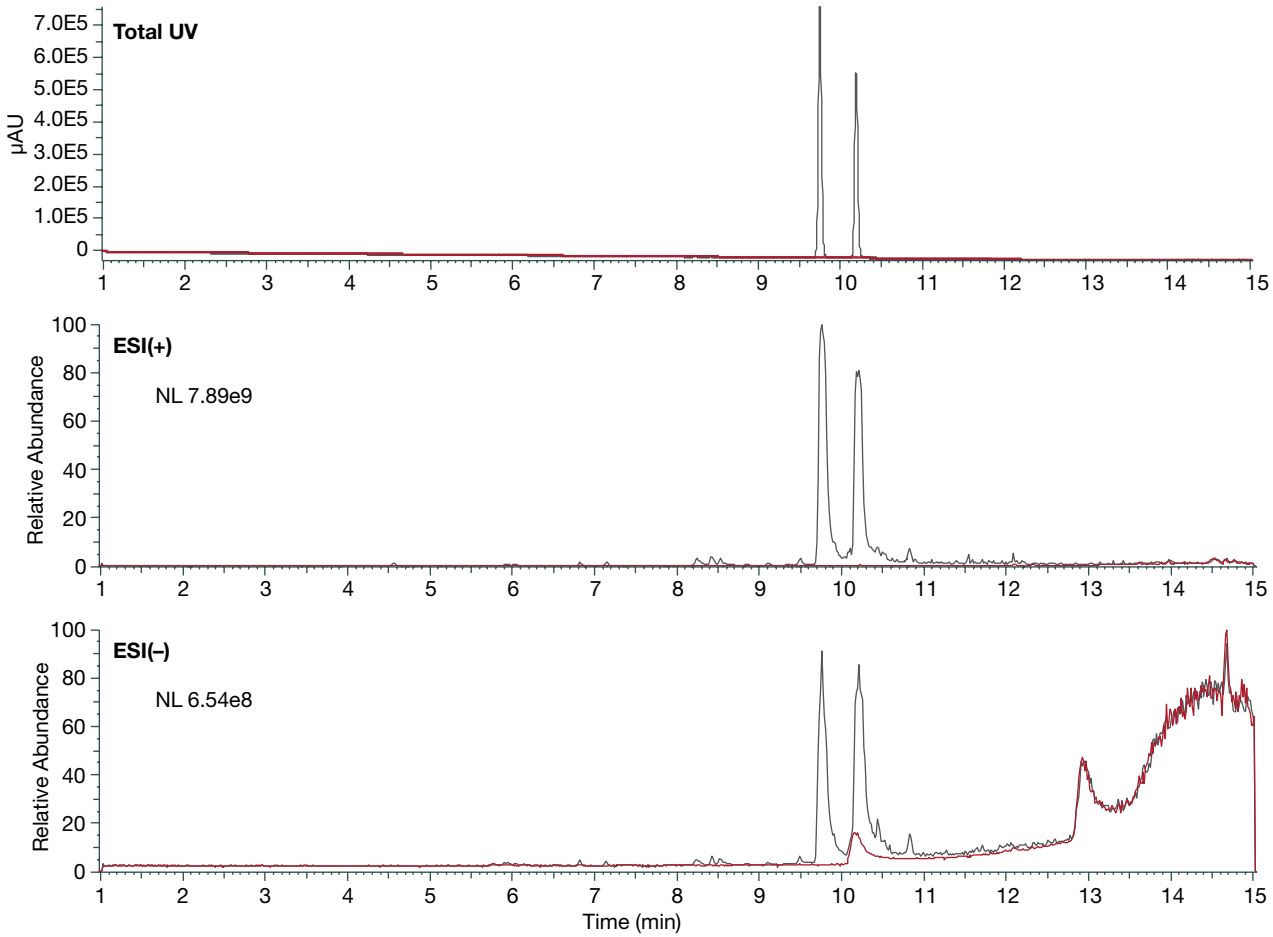

Figure 2. Representative LC/MS chromatograms of 5'-dimethyloxytrityl-2'-O-fluoro-N-benzoyl-adenosine cyanoethyl phosphoramidite (1) from vendor A at 1 mg/mL concentration (gray trace) overlaid with solvent blank injection (red). The expected product is detected as a mixture of diastereomers, due to the chiral center on the P(III) of the phosphoramidite.

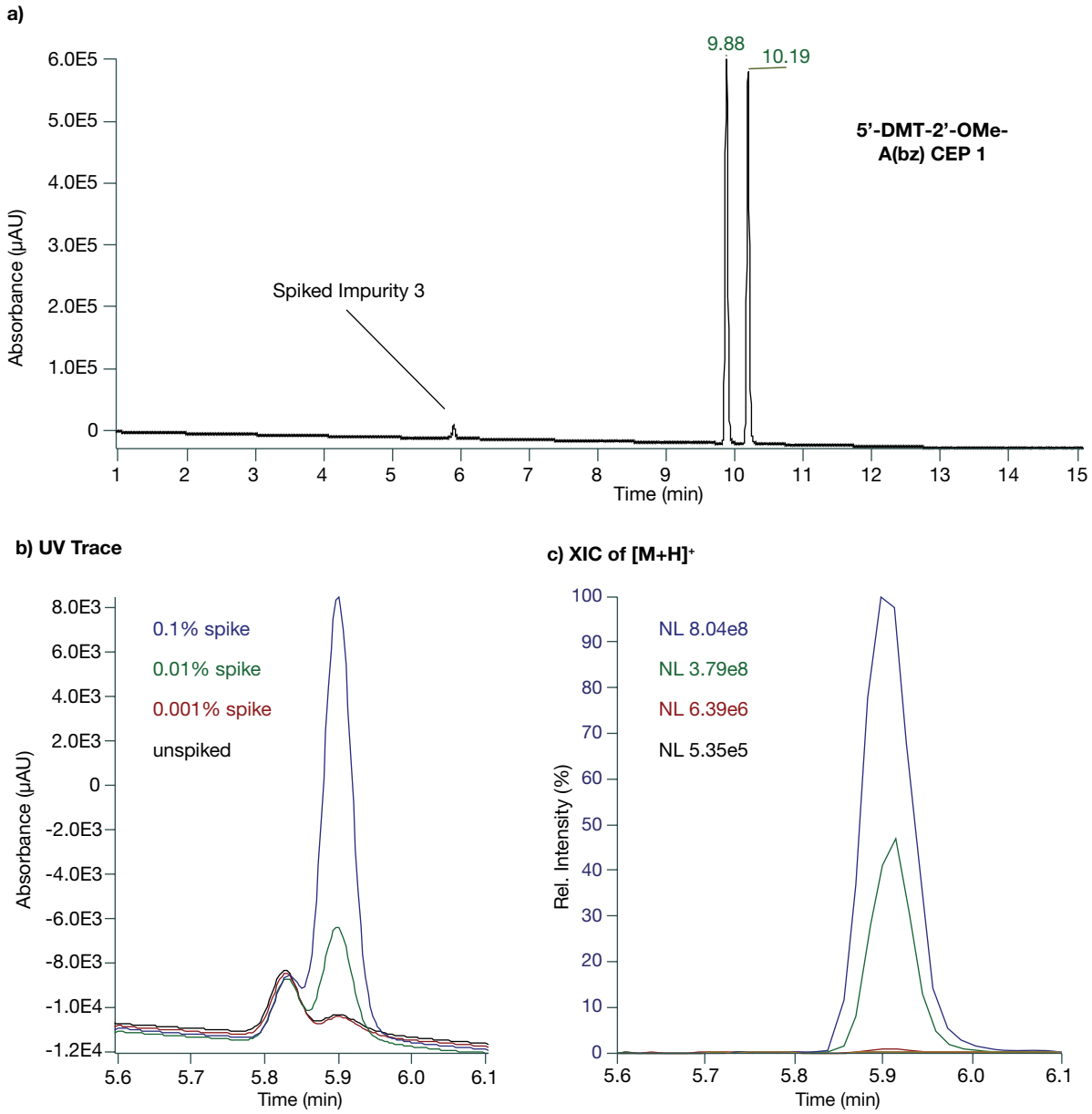

Figure 3. (a) UV chromatogram showing both the spiked impurity 5'-DMT-2'-F-A(bz) (3) and 5'-DMT-2'-OMe-A(bz)-CEP; (b) and (c) UV and ESI(+) XIC of 3, highlighting the sensitive detection of impurities at spiked levels down to 0.01% and 0.001% by UV and MS, respectively

Impurity profiling

After establishing the necessary sensitivity of the method, supplies of 5'-DMT-2'-F-A(bz)-CEP (**1**) obtained from four different vendors were analyzed using the established method. Based on their UV chromatograms, differences in their impurity profiles could readily be observed, as depicted in Figure 4. In this example, twenty-five different impurities were seen in the four vendors' material. The lots contained a combination of many similar impurities as well as some that were unique to specific vendors.

As highlighted by Kiesman *et al.*,[1] the structure and reactivity of the impurities plays a critical role for the oligonucleotide synthesis process beyond the overall purity level of the building blocks. To that end, the data were first processed using the Qualitative workflow in Chromeleon 7.2.10 CDS to automatically detect all peaks in the Total UV spectra present at or above 0.01% relative intensity, after automatic background subtraction of a solvent blank injection. Then, both expected and unexpected (i.e., "untargeted") peak detection of the MS data were carried out using the Compound Discoverer software, allowing the detected UV peaks to be manually correlated to compounds detected in the MS data as shown in Figures 5 and 7a.

Expected compounds were generated by the software based on common transformations including dealkylation, oxidation, reduction, methylation, etc. and combinations thereof from the parent compound, allowing for targeted compound extraction. Meanwhile, untargeted compound detection allowed for the unbiased detection of additional compounds, particularly in cases of substitutions or additions to the parent structure based on their relative abundance compared to a blank sample.

Based on the predicted composition and calculated transformation relative to the parent structure, candidate structures could be proposed for the impurities. Using the acquired MS^2 fragmentation spectra, it was possible to narrow down the possibilities and/or determine the site of transformation to allow confident annotation of the impurities, as detailed hereafter.

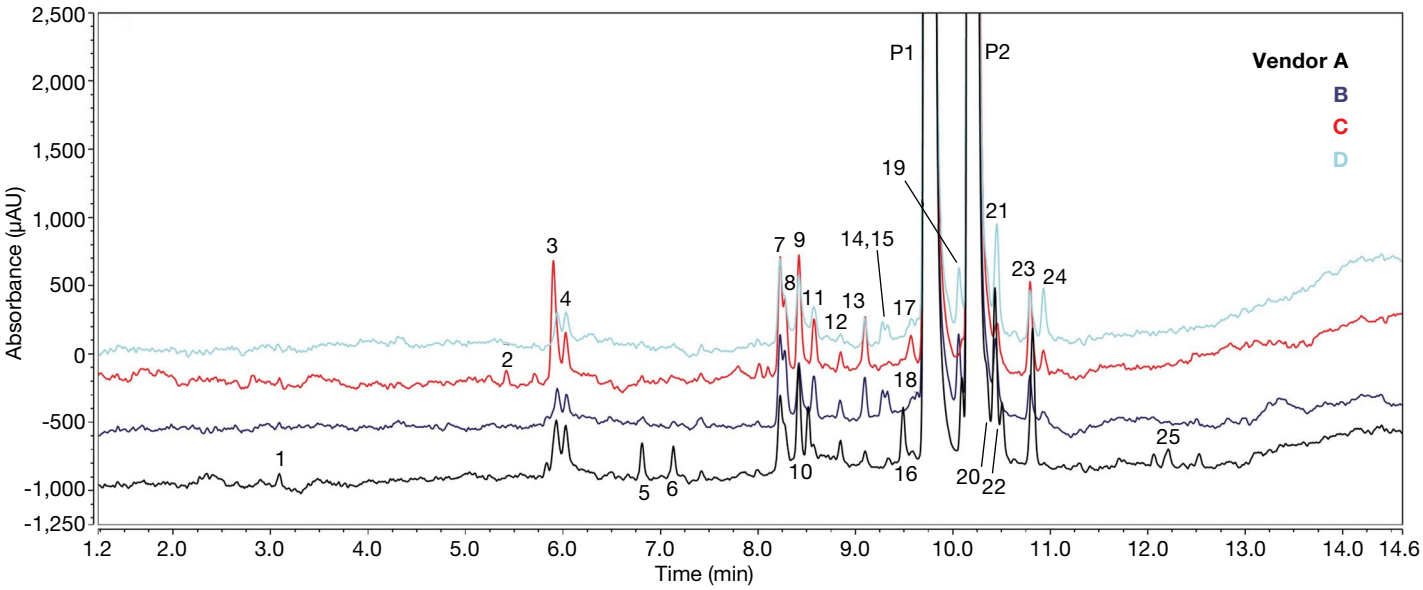

Figure 4. Zoomed-in overlay of total UV chromatograms of 5'-DMT-2'-F-A(bz)-CEP (1) from vendors A (black), B (blue), C (red), and D (light blue) with detected impurities labeled

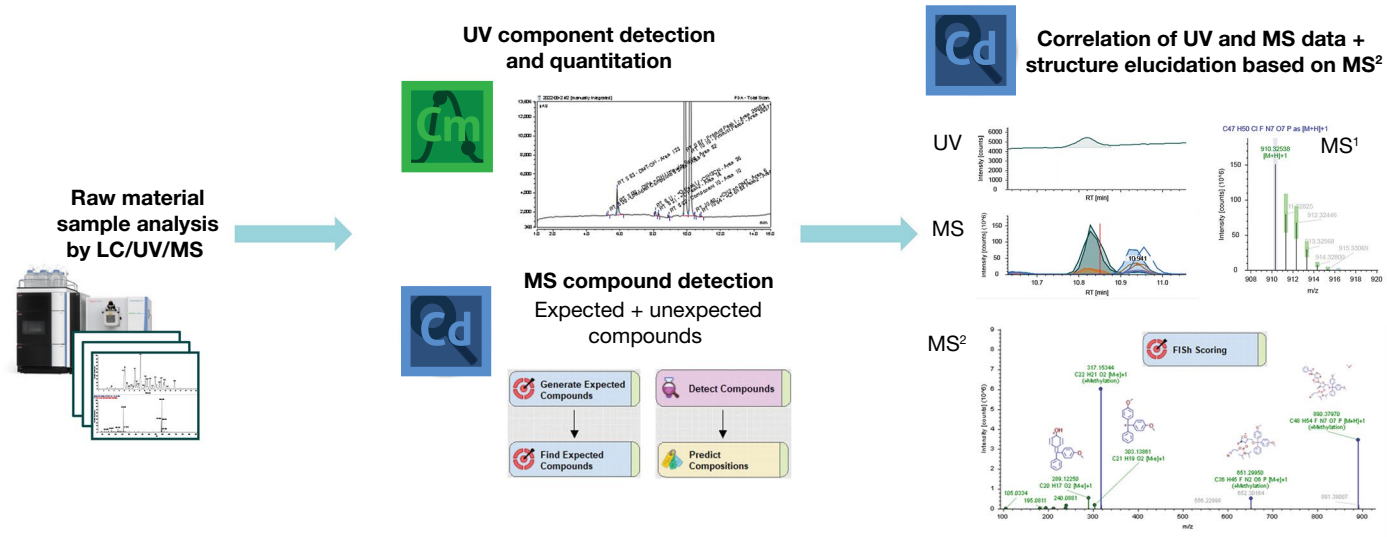

Figure 5. Overview of the impurity detection and identification process based on Chromeleon CDS processing of the UV data and expected and unexpected compound detection and annotation in Compound Discoverer software

Impurity structure elucidation with Compound Discoverer software

The expected compounds workflow used the default transformation list for the “Impurity ID Related and Unknown with Molecular Networks” workflow template including dealkylation and dearylation, as well as (de)hydration, (de)saturation and oxidation and reductions, with methylation added as a custom transformation. The added methylation transformation was detected in Impurity XVII, with an isotope pattern match for the assigned elemental formula, as shown in Figure 6. Additionally, the software automatically generated fragment ion predictions using the FISh algorithm to match the MS^2 fragmentation spectra, with fragment ions matching the parent compound highlighted in green and mass-shifted fragments in blue. Based on this, the methylation could be localized to one of the methoxy groups on the DMT protection group and the impurity classified as *reactive and noncritical,* as the DMT group is removed in the oligonucleotide synthesis cycle.

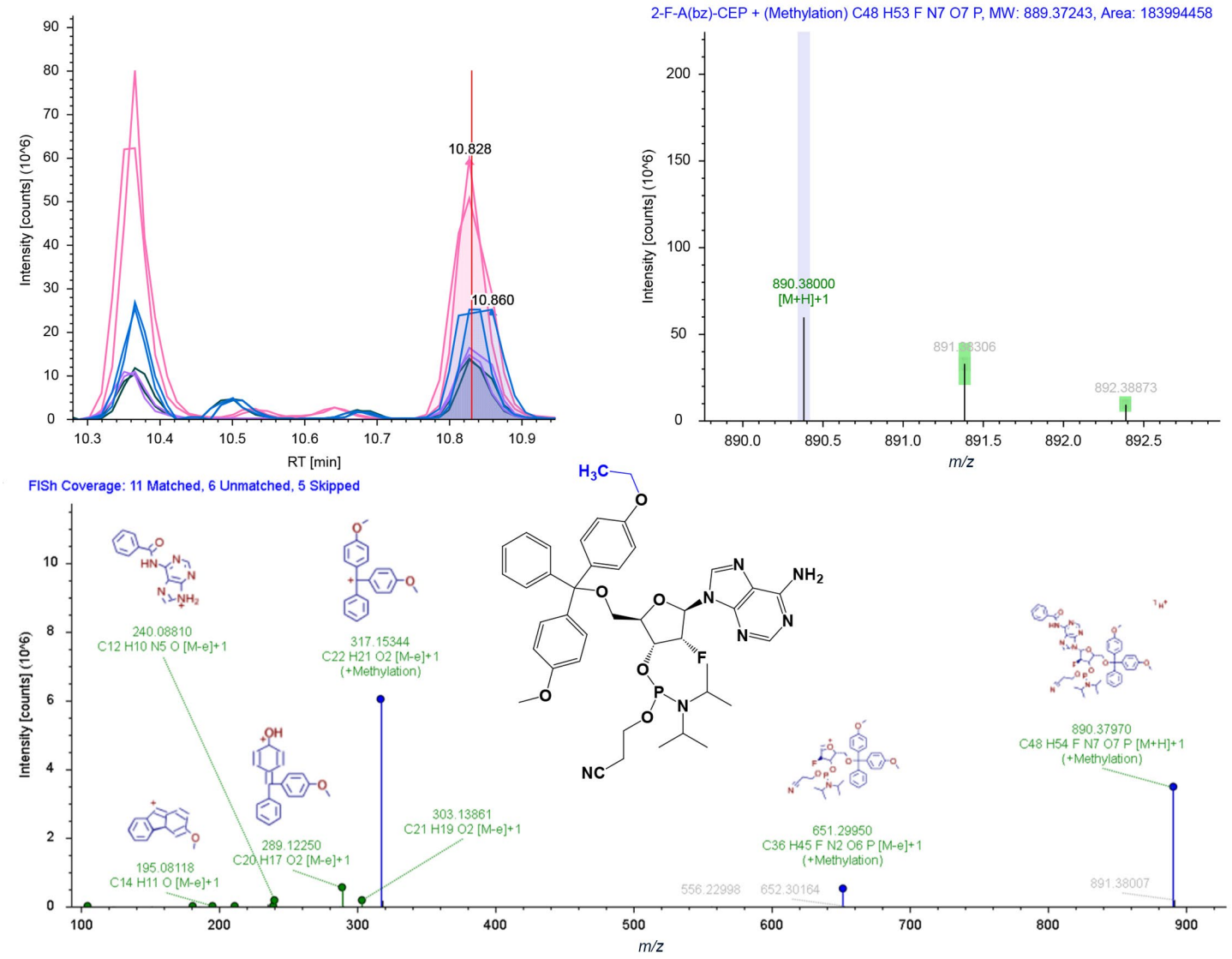

Figure 6. XIC and zoomed MS spectrum of the M+H⁺ ion of the methylated Impurity XVII. The site of methylation could be localized to the DMT group based on the observed shift in the trityl fragment ion to *m/z* 317, and the unshifted ion detected at *m/z* 289 indicates the likely substitution of the methoxy group with ethoxy, resulting in the proposed structure of the impurity in the center.

Using the untargeted workflow in Compound Discoverer software, UV peaks 5 and 6 could be correlated to a compound with a calculated molecular mass of 677.2525 Da (Impurity V), indicative of a diastereomeric P(III) compound. Using the accurate measurement and the isotopic peak pattern, as well as the MS^2 spectrum for the compound, the most likely elemental composition was determined to be $C_{33}H_{37}FN_7O_6P$ with an excellent mass error of -0.30 ppm. This corresponded to a transformation of $-C_{14}H_{14}O$, most likely resulting from the substitution of the DMT group with benzoyl in the 5'-position. This could be confirmed by the absence of the *m/z* 303 fragment in the corresponding fragmentation spectra, as shown in Figure 7d. Based on this structural assignment, impurity V could be classified as *nonreactive and noncritical.*

The importance of fragmentation data for confident structure elucidation is further illustrated by the impurities XVIII and XX, representing multiple isomeric compounds with molecular mass 909.3177 corresponding to chlorine substitution. As highlighted in Figure 8, the chlorine substitution could be localized to either the DMT or benzoyl protecting groups from the shifted fragments present in the MS^2 spectra. For XVIII, a shift corresponding to the chlorination of the benzoyl-protected adenosine base could be observed in comparison to the parent compound fragmentation pattern, as highlighted by the color-coded peak at *m/z* 274 in blue, which was automatically labeled by the Compound Discoverer software. In contrast, for XX, a marked shift of the DMT fragment ion from *m/z* 303 to *m/z* 337 could be observed, indicating that the chlorine substitution is likely a result of impurities in the DMT reagent. As seen in Figure 8b, which labels all observed isomeric impurities based on the site of substitution determined from their respective MS^2 data, the extent of chlorination of the respective protecting groups differs between the four materials analyzed.

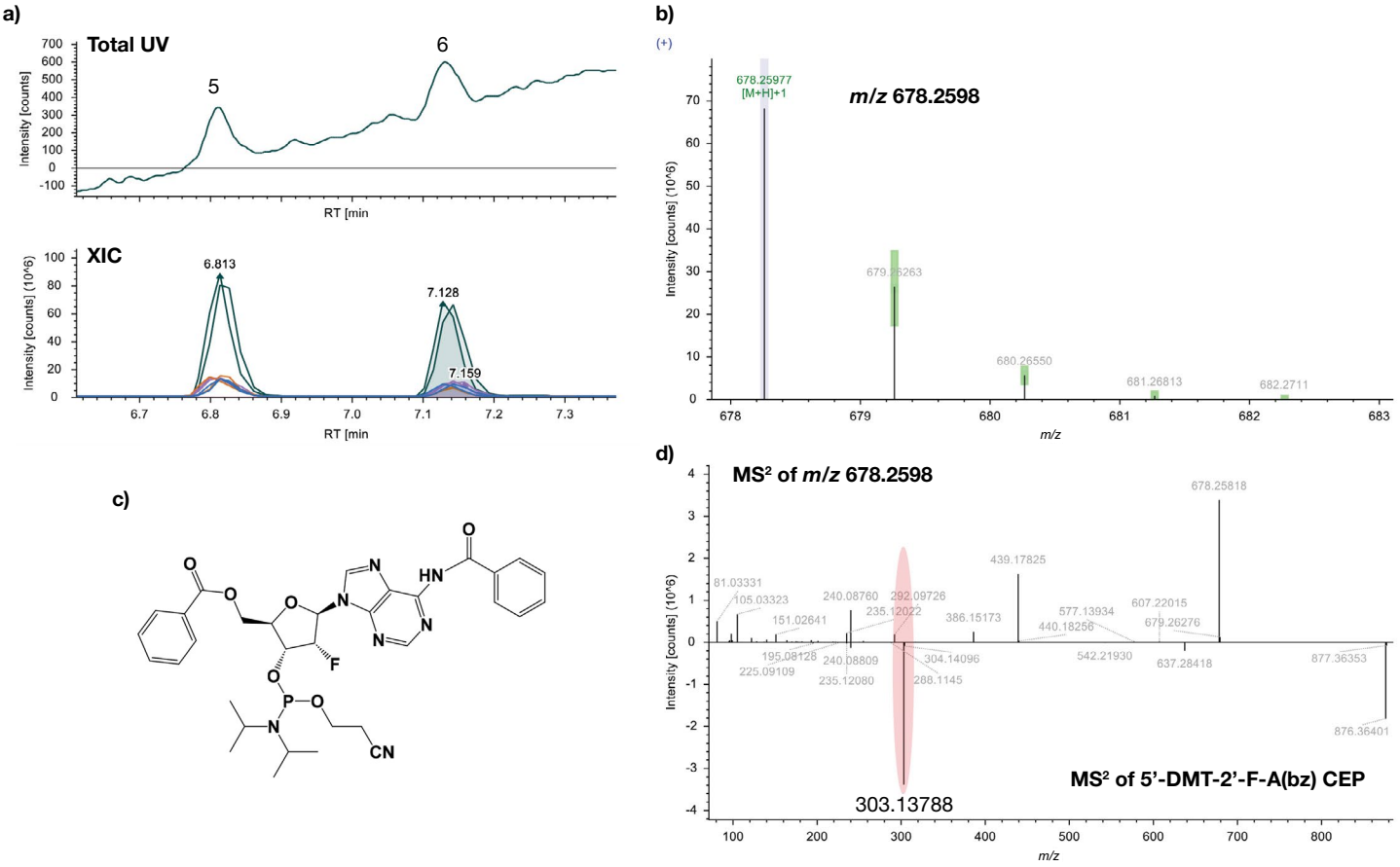

Figure 7. (a) Correlation of peaks 5 and 6 in the total UV chromatogram of 2A with the XIC of *m/z* 678.2598 in Compound Discoverer software; (b) Isotopic peak pattern of the detected compound matching to the elemental composition of $C_{33}H_{37}FN_7O_6P$ within tolerances (green bars); (c) Proposed chemical structure of impurity V based on the combined spectral data; (d) Mirror plot of fragmentation spectrum for impurity V and its parent compound 1, showing the absence of the trityl fragment at *m/z* 303.13788 in the former

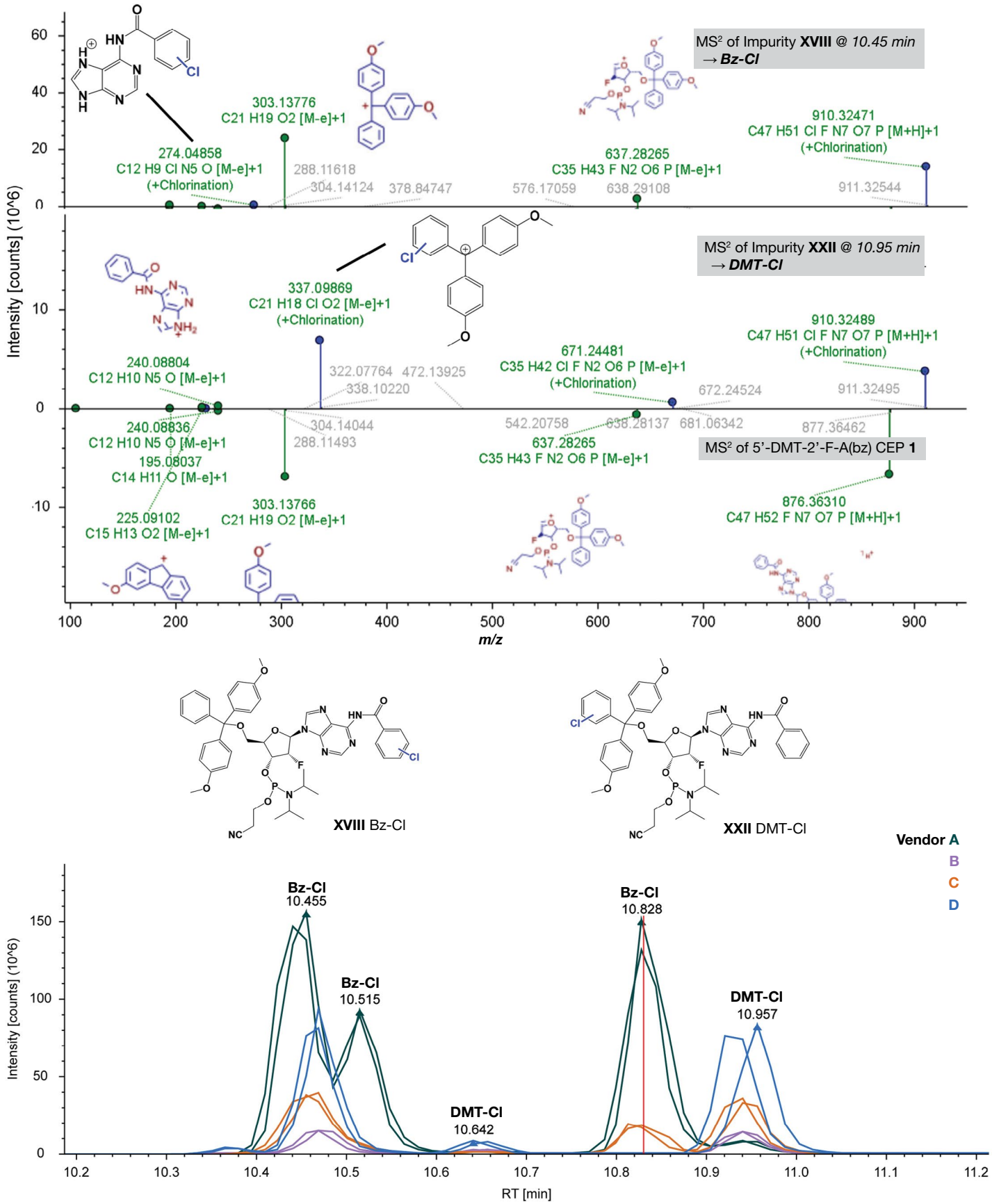

Figure 8. (a) Comparison of the MS² spectra of isomeric impurities XVIII and XX to the expected product 5'-DMT-2'F-A(bz) CEP (2), revealing differences in the fragmentation pattern because of different locations of the chlorine substitution on Bz and DMT, respectively; (b) XIC of the chlorine substitution (MW 909.3177 Da), highlighting the difference in the impurity profiles for the different supplier materials, including other isomeric impurities below the UV detection threshold

Table 5 gives a summary of the detected and identified impurities present in 5'-DMT-2'-F-A(bz)-CEP (1), as elucidated based on their MS data using Compound Discoverer software, with their proposed structures shown in Figure 9.

Table 5. Summary of detected Impurities in 5'-DMT-2'-F-A(bz)-CEP (1) and relative amounts detected in the materials from the different vendors (A–D)

Impurity	UV peak #	RT (min)	MS compound MW (Da)	ΔMW (Da)	Formula	Compound annotation	% of total UV peak area			
							A	B	C	D
I	1	3.1	808.2422	-67.1149	$C_{41}H_{38}FN_6O_9P$	-DIPA +O_2 to P(V) species	0.01%	0.00%	0.00%	0.00%
II	2	5.4	477.2406	-398.1165	*$C_{24}H_{28}ON_9F$*	*Structure not determined (DMT and bz fragments absent in MS²)*	0.00%	0.00%	0.01%	0.00%
III	3	5.9	675.2491	-200.1080	$C_{38}H_{34}FN_5O_6$	-CEP	0.00%	0.00%	0.09%	0.00%
IV	4	6	792.2472	-83.1099	$C_{41}H_{38}FN_6O_8P$	-DIPA + OH	0.07%	0.05%	0.07%	0.05%
V	5+6	6./7.1	677.2525	-198.1046	$C_{33}H_{37}FN_7O_6P$	-DMT +bz	0.05%	0.00%	0.00%	0.00%
VI	7+9a	8.2/8.4	891.3518	15.9947	$C_{47}H_{51}FN_7O_8P$	Oxidation to P(V) species	0.06%	0.10%	0.13%	0.13%
VII	8	8.3	822.3306	-53.0265	$C_{44}H_{48}FN_6O_7P$	HP=O phosphite + loss of cyanoethyl group	0.01%	0.04%	0.04%	0.00%
VIII	9b+10	8.4/8.5	834.2944	-41.0627	$C_{44}H_{44}FN_6O_8P$	substitution of DIPA with iPrOH	0.06%	0.00%	0.00%	0.00%
IX	11a+13a	8.6/9.1	773.3341	-102.0230	$C_{35}H_{50}FN_9O_6P_2$	-DMT +CEP	0.01%	0.05%	0.07%	0.04%
X	11b+13b	8.6/9.1	771.3307	-104.0264	$C_{40}H_{47}FN_7O_6P$	-bz				
XI	12	8.8	779.2753	-96.0818	$C_{45}H_{38}FN_5O_7$	-CEP + bz	0.01%	0.01%	0.01%	0.00%
XII	14+18	9.3/9.6	861.3414	-14.0157	$C_{46}H_{49}FN_7O_7P$	Demethylation on CEP	0.00%	0.03%	0.00%	0.01%
XIII	15	9.3	903.3518	27.9947	$C_{47}H_{55}FN_3O_{12}P$	Acetyl-Methyl substitution on DMT	0.00%	0.01%	0.00%	0.01%
XIV	16	9.5	747.2885	-128.0686	*$C_{42}H_{39}F_2N_5O_6$*	*Structure not determined*	0.03%	0.00%	0.00%	0.00%
XV	17	9.6	992.3551	116.9980	$C_{50}H_{55}FN_8O_9P_2$	-DIPA +CEP	0.00%	0.00%	0.03%	0.00%
XVI	19+21b	10.1/10.4	874.3732	-0.9839	$C_{47}H_{52}FN_8O_6P$	-O +NH on bz	0.08%	0.00%	0.04%	0.00%
XVII	20	10.3/10.8	889.3721	14.0150	$C_{48}H_{53}FN_7O_7P$	Methylation on DMT	0.09%	0.00%	0.00%	0.00%
XVIII	21a+22+23a	10.4/10.5/10.8	909.3177	33.9606	$C_{47}H_{50}ClFN_7O_7P$	Chlorination on bz	0.12%	0.07%	0.05%	0.09%
XIX	23b	10.8	977.3799	102.0228	$C_{59}H_{52}FN_5O_8$	-CEP +DMT	0.02%	0.01%	0.03%	0.02%
XX	24	10.9	909.3177	33.9606	$C_{47}H_{50}ClFN_7O_7P$	Chlorination on DMT	0.00%	0.01%	0.01%	0.04%
XXI	25	12.1/12.2	864.3779	-10.9792	$C_{47}H_{54}FN_6O_7P$	-CN +CH_3 "M-11"	0.02%	0.00%	0.00%	0.00%
P	**P1+2**	**9.8/10.2**	**875.3571**		**$C_{47}H_{51}FN_7O_7P$**	**5'-DMT-2'-F-A(bz)CEP**	**99.35%**	**99.61%**	**99.44%**	**99.61%**

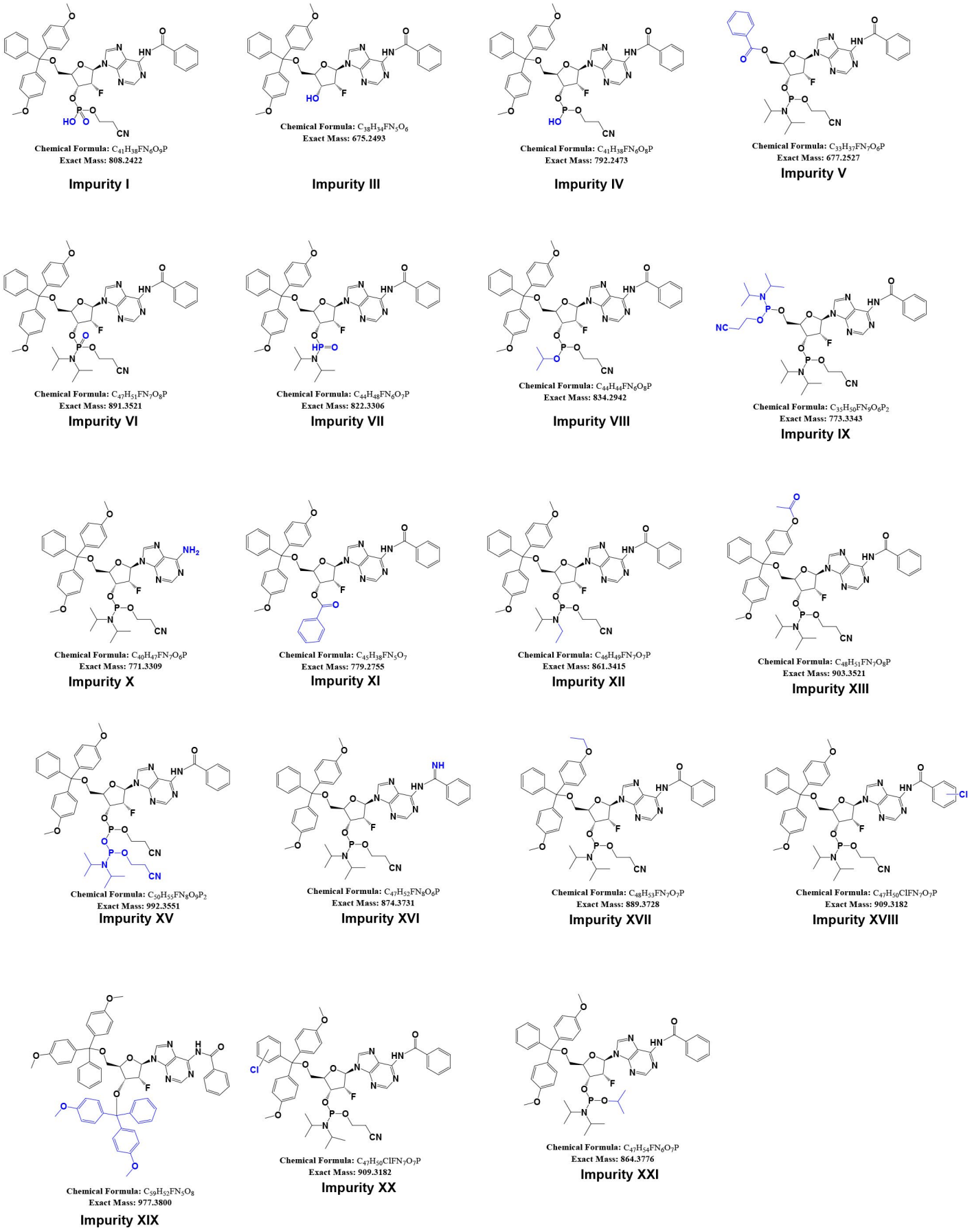

Figure 9. Proposed structures for the detected impurities in 5'-DMT-2'-F-A(bz)-CEP

Conclusion

With the increased interest in therapeutic oligonucleotides, the confident impurity characterization of phosphoramidite building blocks has gained importance. Here, we highlight that the Vanquish Horizon UHPLC system combined with the Orbitrap Exploris 120 mass spectrometer provide excellent sensitivity and high-quality MS data to facilitate the confident identification of phosphoramidite impurities and their profiling across different supplier's materials:

- Sensitive detection of trace impurities at levels of 0.01% and lower was achieved in a spike-in experiment.
- Differences in the impurity profiles of 5'-DMT-2'-F-A(bz)-CEP from different vendors were readily determined, and while all investigated samples showed high purity exceeding the vendors' specification, different levels of impurities that are important to control for in the manufacturing of therapeutic oligonucleotides could be observed.
- Compound Discoverer software automates the mass spectral annotation process from peak detection to elemental composition and transformation prediction and allows localization of transformation sites using FISh fragment ion predictions and labeling of transformation-shifted fragment ions.

References

1. Roy, S.; Caruthers, M. Synthesis of DNA/RNA and Their Analogs via Phosphoramidite and H-Phosphonate Chemistries. *Molecules,* **2013,** *18,* 14268–14284. (doi: 10.3390/molecules181114268)
2. Kiesman, W.F. et al. Perspectives on the Designation of Oligonucleotide Starting Materials. *Nucleic Acid Therapeutics,* **2021,** *31,* 93–113. (doi: 10.1089/nat.2020.0909)
3. ICH, Q3A(R) *Impurities in New Drug Substances* (Feb. 2003) and others.
4. Comstock, K.; Du, M. Impurity profiling of mycophenolate mofetil using an Orbitrap Exploris 120 mass spectrometer and Vanquish Horizon UHPLC combined with Compound Discoverer software. Thermo Fisher Scientific Application Note 000531, 2022.

Learn more at **thermofisher.com/oligonucleotides**